

Article

Formation of Micro- and Nanostructures on the Nanotitanium Surface by Chemical Etching and Deposition of Titania Films by Atomic Layer Deposition (ALD)

Denis V. Nazarov *, Elena G. Zemtsova, Ruslan Z. Valiev and Vladimir M. Smirnov

Received: 9 October 2015; Accepted: 24 November 2015; Published: 2 December 2015

Academic Editor: Peter J. King

Institute of Chemistry, Saint Petersburg State University, Universitetskii pr. 26,
Saint Petersburg 198504, Russia; ezimtsova@yandex.ru (E.G.Z.); rzvaliev@mail.rb.ru (R.Z.V.);
vms11@yandex.ru (V.M.S.)

* Correspondence: dennazar1@yandex.ru; Tel.: +7-812-324-12-70 (ext. 56-46); Fax: +7-812-428-93-41

Abstract: In this study, an integrated approach was used for the preparation of a nanotitanium-based bioactive material. The integrated approach included three methods: severe plastic deformation (SPD), chemical etching and atomic layer deposition (ALD). For the first time, it was experimentally shown that the nature of the etching medium (acidic or basic Piranha solutions) and the etching time have a significant qualitative impact on the nanotitanium surface structure both at the nano- and microscale. The etched samples were coated with crystalline biocompatible TiO₂ films with a thickness of 20 nm by Atomic Layer Deposition (ALD). Comparative study of the adhesive and spreading properties of human osteoblasts MG-63 has demonstrated that presence of nano- and microscale structures and crystalline titanium oxide on the surface of nanotitanium improve bioactive properties of the material.

Keywords: atomic layer deposition (ALD); chemical etching; nanostructured titanium; titanium implants; titania coatings

1. Introduction

Titanium and its alloys have a unique combination of acceptable mechanical properties and biocompatibility that allows it to be widely used in medical practice as a material for implants for the past 50 years [1–4]. Recently, interest to ultrafine-grained titanium (nanotitanium) in the field of biomedical materials was increased due to its excellent mechanical properties [5–7]. However, the mechanical properties are not the only characteristic that determines the success of the use of certain materials in the field of implantology. Other important characteristics of the material are its bioinertness, biocompatibility and bioactivity [1–3]. The transition to the production of materials based on nanotitanium and bioactive nanocoating is one of the backbone approaches to the synthesis of the new class of biomaterials that are widely used in modern dentistry, reconstructive surgery and orthopedics [2–4,8,9]. It should be noted that the improvement of the properties of the biomedical material requires the control of not only the chemical properties (primarily composition of the surface) but also surface properties (crystallinity, morphology and relief). Recent works showed that the presence of the structures at both micro- and nanoscale can give a significant contribution to the biocompatibility of the implants [10]. The micro- or nanoscale structures (developed relief) are usually achieved by machining, chemical or electrochemical etching [11,12].

It is currently generally recognized that the nanotitanium bioactivity can be improved by bioactive titanium dioxide coating [1,2,10,11,13]. Typically, for the production of coatings based on

oxides, including preparation of titanium dioxide films, the following methods are used: anodic oxidation [14,15], plasma spraying [16,17], chemical vapor deposition [18], sol-gel [19,20], and others [11,19]. However, these methods in most cases do not allow obtaining a uniform coating on the developed relief surface and porous materials with preservation of their topography. One of the most acceptable and productive methods to create a continuous and uniform coating on the surface of such supports is the atomic layer deposition (ALD) [21].

ALD is based on the cyclic self-limiting gas-solid chemical reactions on the substrate surface whereby the film growth process takes place layer by layer [21]. While increasing number of surface chemical reaction (number of ALD cycles), the film thickness increases as well. In this way, the films of carbides, nitrides, sulfides, and metal film [22,23] can be obtained, but the method most widely used for the deposition of oxides [21,22,24–26]. ALD has two main advantages: high precision of the films thickness and high uniformity of the coating on the surface of planar and porous substrates [21,27,28]. Due to these features, ALD is widely used for the deposition of the films in the semiconductor industry [29], catalysis [30], solar energy [31], Li-ion batteries and supercapacitors [32]. Despite the advantages of the method, ALD has not yet found a wide application in the field of coatings for biomedical materials in general, and medical implants in particular. There are only a few papers devoted to the deposition of biocompatible coatings for implantology by ALD [13,33–36]. Undoubtedly this trend is very promising, and requires more detailed study.

In this paper, we demonstrate the opportunity of the integrated approach for creation of new implant material. The approach combines advantages of the methods described above. Severe plastic deformation (SPD) method improves mechanical properties of the material. Chemical etching produces a structure and morphology of the surface that is necessary for the successful and rapid engraftment of the implant. Finally, ALD method served for deposition of biocompatible and bioactive crystalline titania coating that protects implant from biological corrosion, keeps the etched titanium surface structure and favors the growth of bone tissue.

2. Experimental Section

2.1. Fabrication of Micro- and Nanoscale Structures on the Nanotitanium Surface by Controlled Liquid Phase Chemical Etching

Nanotitanium samples were prepared in Limited Liability Company “Nanomet”, Ufa, Russia, from titanium Grade 4. Titanium rods of 1 m length were subjected to Equal-Channel Angular Pressing by ECAP-Conform processing at 400 °C for 5 passes. The value of accumulated true strain was 3.5. Detailed description of ECAP-Conform processing technique can be found in [37]. After ECAP-Conform processing, the billets were subjected to drawing at 200 °C resulting in production of rods with a diameter of 6 mm. The average grain size of nanotitanium was ~50–100 nm. Samples before etching were treated by machining. Firstly, nanotitanium rod was cut into discs having thickness of 2–3 mm by the Buehler IsoMet 1000 machine (Buehler, Lake Bluff, IL, USA). Then, these discs were ground and polished by semiautomatic machine Buehler MiniMet 1000 (Buehler, Lake Bluff, IL, USA) to mirror-like surface (roughness less than 5 nm). Then the nanostructured titanium discs were cleaned in ultrasonic bath in acetone and deionized water for 15 min. Finally the samples were dropped into a basic ($\text{NH}_4\text{OH}/\text{H}_2\text{O}_2$) or acidic ($\text{H}_2\text{SO}_4/\text{H}_2\text{O}_2$) Piranha solution at room temperature. The ratio of reactants was 7/3; exposure times were 15 min, 2 and 24 h for both types of etching media. Immediately after etching the samples were taken out of the etchant and thoroughly washed in distilled water and acetone using an ultrasonic bath.

2.2. Synthesis of Titanium Oxide Nanostructures by ALD on the Surface of Chemically Etched Nanotitanium

Titanium oxide coatings were obtained by ALD on the surface of the polished, etched nanotitanium and monocrystalline silicon plates (100) that act as a witness for ellipsometry and X-ray reflectometry (XRR) measurements. The deposition was performed at the commercial

“Nanoserf” setup (Nanoengineering Ltd., St. Petersburg, Russia) in the Resource Center “Innovative technologies of composite nanomaterials” Saint Petersburg State University (SPbSU). The deposition was performed in hot-wall, flow-type reactor having slot-type geometry. Base pressure of the reactor is 6.5 Pa. Nitrogen with purity of 99.9999% was used as carrier and purging gas. Titanium isopropoxide (Sigma Aldrich, St. Louis, MO, USA, 99.999%) was supplied into a reaction chamber as a solution in isooctane by the injection valve. Isooctane acted as a carrier gas, which evaporates quickly after injection into the hot reactor and due to isooctane chemical properties it does not cause adverse chemical reactions. Volume ratio of the titanium isopropoxide/isooctane was 1/20. Flowrate of the titanium isopropoxide for one cycle was about 4 μmol , and the pulse duration was 20 ms. Water source was delivered by vapor with the water ampoule being held at 27 °C, pulse duration was 500 ms. Deposition was carried out as follows: Before precursor pulse the supply of inert gas was stopped and the reactor was evacuated for 5 s to a pressure of about 0.7 hPa. Then reagent was pulsed and held without pumping and purging for 0.5 s (static mode). Since the vapor pressure of the reagent considerably higher than the pressure inside the reactor (0.7 hPa), the precursor expands and occupies all the volume of the reactor. After that, pumping occurred within 5 s to remove the reaction products and excess reactants. Then, a purge pulse proceeded at a pressure of 25 hPa for further removal of reagents during 20 s. Thus, the overall purge stage lasted 30 s. Reactor pressure at water and titanium isopropoxide solution pulse increased to 30 and 45 hPa respectively. The temperature of the reactor chamber was maintained at 250 °C. Total reactor gas flow at purge pulse was 300 sccm (standard cubic centimeters per minute). Applied number of ALD cycles was 400 and thickness was 20 nm, which corresponds to TiO_2 growth rate 0.05 nm/cycle.

2.3. The Study of Morphology, Relief, Structure and Composition

The thickness of TiO_2 film deposited on the surface of silicon witness and polished non-etched nanotitanium was determined by the spectral ellipsometry and X-ray reflectometry (XRR). The ellipsometry instrument (Ellips-1891 SAG, Novosibirsk, Russia) provided an accuracy of the film thickness determination of 0.3 nm in the thickness range of 1–100 nm. X-ray reflectometry (XRR) and X-ray diffraction studies (XRD) in both symmetrical $\theta/2\theta$ and asymmetrical surface sensitive grazing incidence (GID) modes were performed using a Bruker D8 DISCOVER high-resolution diffractometer (Bruker, Billerica, MA, USA) and analyzed with TOPAS 4.2 (XRD) and LEPTOS 7.7 (XRR) software at the Resource Centre “X-ray Diffraction Studies” SPbSU.

The topography of the samples surfaces was studied using a Solver P47 Pro (NT-MDT, Moscow, Russia) probe microscope in the tapping mode via atomic force microscopy (AFM). The AFM study was conducted at 3–4 points on the surface of the sample. Scanning electron microphotographs were obtained using the SEM Zeiss Merlin at the “Nanotechnology” Interdisciplinary Resource Centre SPbSU. Microscope spatial resolution was of around 1 nm and magnification up to 200 k \times . In-lens SE and SE2 regimes was used.

X-ray photoelectron spectra were registered with a “Thermo Fisher Scientific Escalab 250Xi” spectrometer (Thermo Fisher, Waltham, MA, USA) at the Resource Centre of “Physical Methods of Surface Investigation” SPbSU. The samples were excited by Al $K\alpha$ (1486.7 eV) X-rays in a vacuum of 7×10^{-8} Pa. The sample charging was automatically compensated. The binding energy scale has been referenced using the C1s carbon line (284.8 eV) [38].

2.4. Adhesive and Spreading Properties of the Human Osteoblasts MG-63 on the Titania Nanostructured Surface

Adhesion properties and the rate of the cells growth of the human osteoblasts have been evaluated using scanning electron microscopy (SEM). For this purpose, titanium samples treated by the cells have been used. The study is performed in the Institute of Cytology (RAS, St. Petersburg, Russia). The following samples were investigated:

Sample 1—Polished coarse grained titanium; Sample 2—Polished nanotitanium; Sample 3—Nanotitanium etched in basic Piranha for 15 min; Sample 4—Nanotitanium etched in basic Piranha for 15 min with subsequent deposition of titania (thickness of the layer is 20 nm); Sample 5—Nanotitanium etched in acid Piranha for 15 min; and Sample 6—Nanotitanium etched in acid Piranha for 15 min with subsequent deposition of titania (thickness of the layer is 20 nm).

All the samples have been placed into the Petri dishes and sterilized by means of ozonation. Cell line MG-63 has been spread onto the surface from 100 μL nutrient solution in the manner that the non-flowing drop is formed. The cell concentration was $1 \times 10^5/\text{cm}^2$ of the sample. The samples so coated with cells suspension are treated in the conditions of CO_2 -incubator at 37°C for 3 h. This time is supposed to be enough for the cells adhesion on the samples surfaces. After that, nutrient solution has been added to the Petri dishes. In the control experiment, cell suspension has been spread onto the surface of the cultural dish.

After 5 days of cultivation, nutrient solution has been removed, washed three times with phosphate buffer saline (PBS) and fixed in the 20-fold volume of 2.5% solution of glutaric aldehyde. Scanning electron microscopy (JSM-35.7, Tokyo, Japan) has been used for the evaluation of the state of cells (*i.e.*, the adhesion and spreading modes of the cells on the samples surfaces).

3. Results and Discussion

3.1. Chemical Etching, Composition, Morphology and Surface Relief

According to [11,39] the surface topography of the titanium greatly varies during the etching process. The morphology mainly depends on the nature of the etchant. Acidic etchant (sulfuric or fluorosulfonic acid) forms spongy structure, processing of trifluoroacetic acid results in the formation of large (up to microns in a diameter and 100 nm in depth) craters, whereas alkaline etchants (aqueous ammonia) gives the network structure, the mesh size ranges depending on the concentration of the etchant [39]. The use of the chemical etching method for controlling the surface roughness is described in more detail in reviews [11,40]. However, the information on the etched nanostructured titanium has almost not represented until now. Thus, the first step of the work was a brief study of the effect of the nature of etchant and etching time on the relief, structure and surface morphology of the nanotitanium.

As etchants we choose the acidic ($\text{H}_2\text{SO}_4/\text{H}_2\text{O}_2$) and basic ($\text{NH}_4\text{OH}/\text{H}_2\text{O}_2$) Piranha solutions. These solutions are widely used for cleaning and hydrophilization of the surface of various materials and with respect to metal materials and particularly for titanium this solution can act as etchants [39]. Selecting the regime of etching (time and concentration of etchant) we were guided by the data for coarse grained titanium [39], as well as our previous studies devoted to etching of the nanotitanium in HF and HF + HNO_3 solutions [41].

Figure 1 shows the SEM images (magnification of 200 k \times) of the samples after etching in acidic and alkaline Piranha solutions at exposures of 15 min, 2 h and 24 h. SEM data indicate that the etching in the acidic Piranha in the range from 15 min to a few hours leads to “sponge” nanoscale structure, which is destroyed at longer exposures (about 24 h). The formation of such structures is also characteristic of coarse grained titanium [39]. Alkaline Piranha solution acts in the different manner; the sample after a 15 min treatment is characterized by “coral” structure. The appearance of “coral” structure is likely to be caused by etching in the first place on the grain boundaries. Thus, the result of this etching is the appearance of grains of nanostructured titanium. By increasing the etching time to 2 h, etching character is changed. In this case, firstly nanotitanium grains are etched and the grain boundaries only remain on surface of the sample. Changes in the nature of etching are likely due to the gradual oxidation and passivation of the titanium grain boundaries. Thus, the 2 h etching results in a “mesh” structure of the surface, which has the size of the grid comparable to nanotitanium grain size (50–100 nm). A further increase in etching time leads to the formation of a disordered “sponge” structure.

The SEM data at magnification of 10 k \times (Figure 2) shows that the etching in H₂SO₄/H₂O₂ leads to noticeable changes in morphology on microscale at exposure time close to 24 h. The changes manifest themselves in the presence of randomly distributed structures with irregularly shape. Etching in NH₄OH/H₂O₂ leads to the formation of the pits with a diameter of 1–2 μ m. A marked degree of this microscale structures is observed when expose time is more than 15 min and it reaches the maximum number when exposing time is about 2 h.

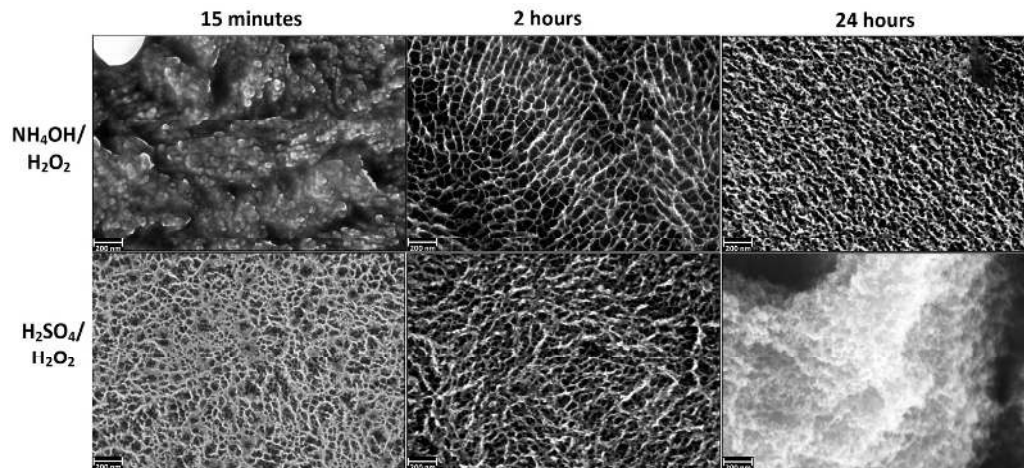


Figure 1. Characteristic scanning electron microscopy (SEM) images of nanotitanium etched in NH₄OH/H₂O₂ and H₂SO₄/H₂O₂ solutions during 15 min, 2 h and 24 h (magnification: 200 k \times , scale bar: 200 nm).

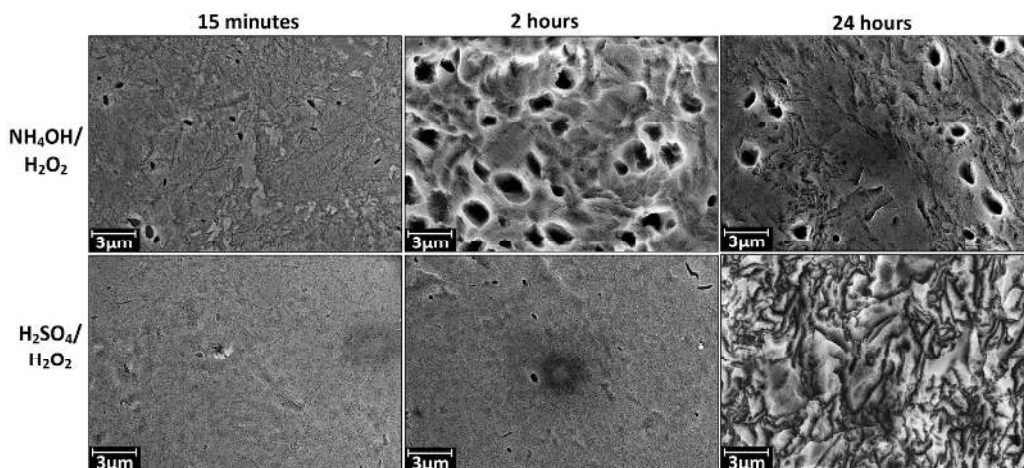


Figure 2. Characteristic SEM images of nanotitanium etched in NH₄OH/H₂O₂ and H₂SO₄/H₂O₂ solutions during 15 min, 2 h and 24 h (magnification: 10 k \times , scale bar: 3 μ m).

Analysis of the AFM data on the scale of 1 \times 1 μ m² (Figure 3) and 10 \times 10 μ m² (Figure 4) showed a significant difference the surface topography of the sample NH₄OH/H₂O₂-15 min etching (“coral” structure) from the rest. The values of the mean-square roughness (RMS) naturally increase with increasing exposure time (from 15 min to 24 h). This values increase from 3.9 to 29 nm for H₂SO₄/H₂O₂ and from 7.3 to 9.2 nm for NH₄OH/H₂O₂. RMS of the initial polished nanotitanium equals to 2.6.

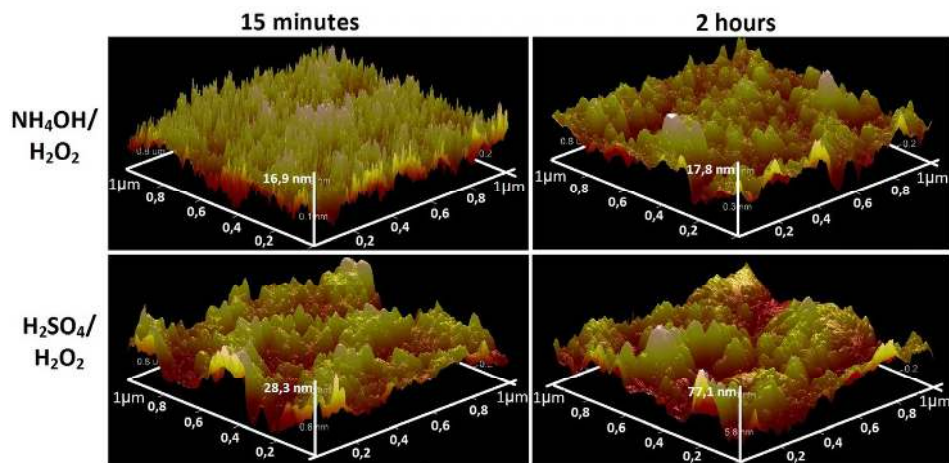


Figure 3. Atomic force microscopy (AFM) topographies ($1 \times 1 \mu\text{m}^2$) of the surface of nanotitanium etched in $\text{NH}_4\text{OH}/\text{H}_2\text{O}_2$ and $\text{H}_2\text{SO}_4/\text{H}_2\text{O}_2$ solutions during 15 min and 2 h.

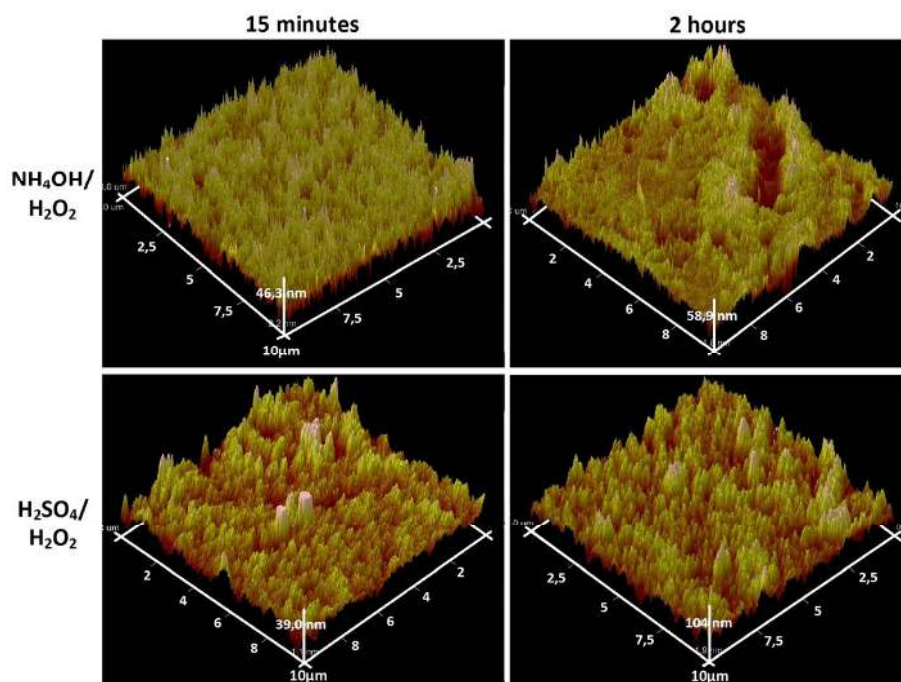


Figure 4. AFM topographies ($10 \times 10 \mu\text{m}^2$) of the surface of nanotitanium etched in $\text{NH}_4\text{OH}/\text{H}_2\text{O}_2$ and $\text{H}_2\text{SO}_4/\text{H}_2\text{O}_2$ solutions during 15 min and 2 h.

In summary, the SEM and AFM data show opportunity for creation of the developed relief on the nanotitanium surface by chemical etching in Piranha solutions. It is worth noting that the relief has various type of morphology (“coral”, “mesh”, “sponge”, “micropits”) both at nano- and microscale.

The study of the composition of the surface of the etched samples by X-ray photoelectron spectroscopy (XPS) showed the presence of Ti, O and C. The carbon contamination seemingly is caused by adventitious atmospheric hydrocarbon on the surface of the samples [38]. No other contaminants of the samples surface were found. It should be noted that the peak of Ti^0 (453.9 eV) reduces or disappears after etching (Figure 5). This fact indicates that the oxidation accompanies the etching.

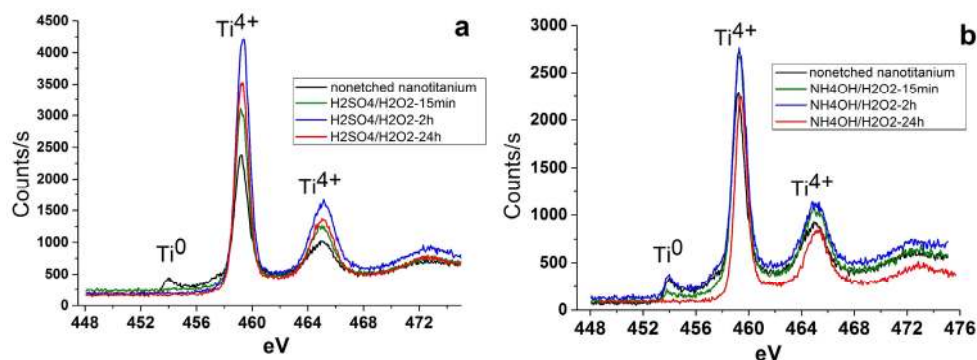


Figure 5. X-ray photoelectron Ti2p level spectra of nanotitanium etched in (a) acidic Piranha and (b) basic Piranha.

3.2. Deposition of TiO₂ Nanocoatings, Structure, Composition and Morphology

It is known [11,12] that the natural oxides and oxides produced during etching cannot fully prevent the implant material from corrosion in aggressive biological environment. Thus, additional protective layers should be deposited on the implant surface. It is to be noted that the degree of crystallinity surface oxide layer of the titanium implants significantly affects on engraftment of bone tissue [13]. Higher crystallinity leads to more favorable growth of hydroxyapatite (the main inorganic component of bone tissue) [42]. Rutile exhibits the most suitable crystalline structure, however, it is seen from experimental data that rutile does not demonstrate significant advantage at *in vitro* medical experiments in comparison to anatase [43]. On the contrary, anatase film enhances osteoblast adhesion, spreading and proliferation by affecting surface contact angles and/or wettability [42].

In connection with the above, an important task for our research was to produce polycrystalline films of titanium dioxide. The main parameters that influence on the film crystallinity are the deposition temperature and the layer thickness. According to the literature data [22] crystalline films are obtained at temperatures of 225 °C and above, but thickness of the film/number of ALD cycles is 12 nm/300 cycles [13]. In this regard, nanofilms of crystalline titanium dioxide on the surface of the etched nanotitanium were synthesized at a temperature of 250 °C for 400 cycles. Indeed, preliminary deposition showed that the films obtained after 400 ALD cycles and at a temperature 250 °C are polycrystalline and have the anatase structure (Figure 6).

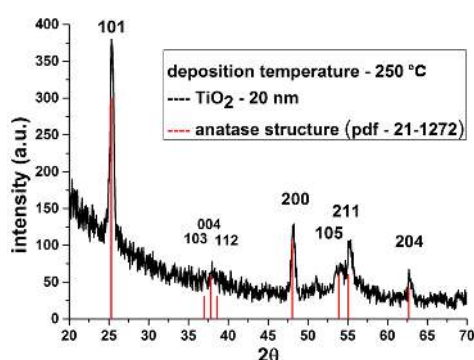


Figure 6. X-ray diffraction studies (XRD) patterns of TiO₂ coatings deposited on titanium substrates at 250 °C.

Based on the SEM and AFM data, we chose the following samples for TiO₂ deposition:

- (1) NH₄OH/H₂O₂-15 min—“coral” structure.
- (2) NH₄OH/H₂O₂-2 h—“mesh” structure.

- (3) $\text{H}_2\text{SO}_4/\text{H}_2\text{O}_2$ -15 min—“sponge” structure.
- (4) $\text{H}_2\text{SO}_4/\text{H}_2\text{O}_2$ -24 h—disordered, developed relief.

Since the determination of the thickness of the films on porous objects by spectroscopic ellipsometry and XRR methods is almost impossible the silicon wafer (the witness) was placed in the reactor near to the titanium samples. Spectroscopic ellipsometry and XRR showed the TiO_2 film thickness of about 20 nm.

The SEM data (Figure 7) suggest that nanoscale relief is saved only for the sample $\text{NH}_4\text{OH}/\text{H}_2\text{O}_2$ -15 min (Figure 7a)—“coral” structure. This fact is quite expected, as the size of the nanostructures after etching does not exceed a few tens of nanometers. Thus, after the deposition of films, the nanostructures are overgrown by layer of titanium dioxide.

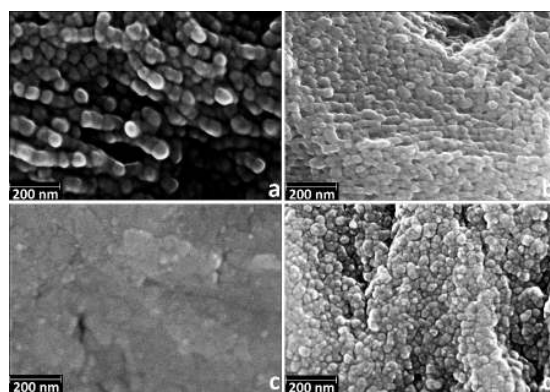


Figure 7. Characteristic SEM images of nanotitanium etched in Piranha solutions and TiO_2 coated by ALD (magnification: 200 k \times , scale bar: 200 nm) (a) $\text{NH}_4\text{OH}/\text{H}_2\text{O}_2$ -15 min; (b) $\text{NH}_4\text{OH}/\text{H}_2\text{O}_2$ -2 h; (c) $\text{H}_2\text{SO}_4/\text{H}_2\text{O}_2$ -15 min; and (d) $\text{H}_2\text{SO}_4/\text{H}_2\text{O}_2$ -24 h.

In general, all the samples after deposition demonstrate the presence of the grains of 30–100 nm in diameter. It is worth noting that grains packing of nanotitanium etched in $\text{NH}_4\text{OH}/\text{H}_2\text{O}_2$ is much higher after 2 h than after 15 min. For the samples after $\text{H}_2\text{SO}_4/\text{H}_2\text{O}_2$ etching, grains appear with the increased etching time.

Note that the coating preserves initial relief of the etched nanotitanium at the micro scale. However, we found some healing of micrometer holes that is indicative for the sample $\text{NH}_4\text{OH}/\text{H}_2\text{O}_2$ -2 h (Figure 8b) and, oppositely, appearance of such holes for $\text{H}_2\text{SO}_4/\text{H}_2\text{O}_2$ -24 h (Figure 8d).

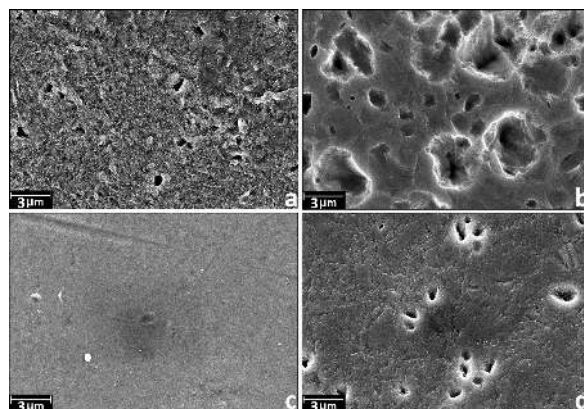


Figure 8. Characteristic SEM images of nanotitanium etched in Piranha solutions and TiO_2 coated by atomic layer deposition (ALD) (magnification: 10 k \times , scale bar: 3 μm) (a) $\text{NH}_4\text{OH}/\text{H}_2\text{O}_2$ -15 min; (b) $\text{NH}_4\text{OH}/\text{H}_2\text{O}_2$ -2 h; (c) $\text{H}_2\text{SO}_4/\text{H}_2\text{O}_2$ -15 min; and (d) $\text{H}_2\text{SO}_4/\text{H}_2\text{O}_2$ -24 h.

The study of the surface composition of TiO₂ coated samples by XPS showed only the presence of Ti, O and C. Note that the complete disappearance of the Ti⁰ peaks is observed for all films (Figure 9). This observation confirms the full coverage of the surface of the sample by continuous TiO₂ layer.

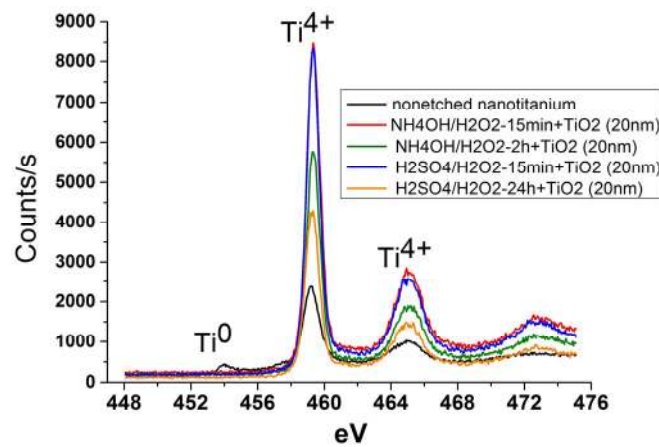


Figure 9. X-ray photoelectron Ti2p level spectra of nanotitanium etched in Piranha solutions and TiO₂ coated by ALD.

3.3. Adhesive and Spreading Properties of the Human Osteoblasts MG-63

To investigate the biocompatibility of biomedical implant surfaces, a number of analytical methods exist to assess cellular responses. The methods include the study of the cell adhesion, proliferation, migration, differentiation and cell survival. Adhesion and spreading are the initial and necessary steps in the process of bone healing. Thus, adhesive and spreading properties give initial information on biocompatibility and bioactivity of the implant. We applied these methods to study cellular responses. Results of the study are presented at Figure 10.

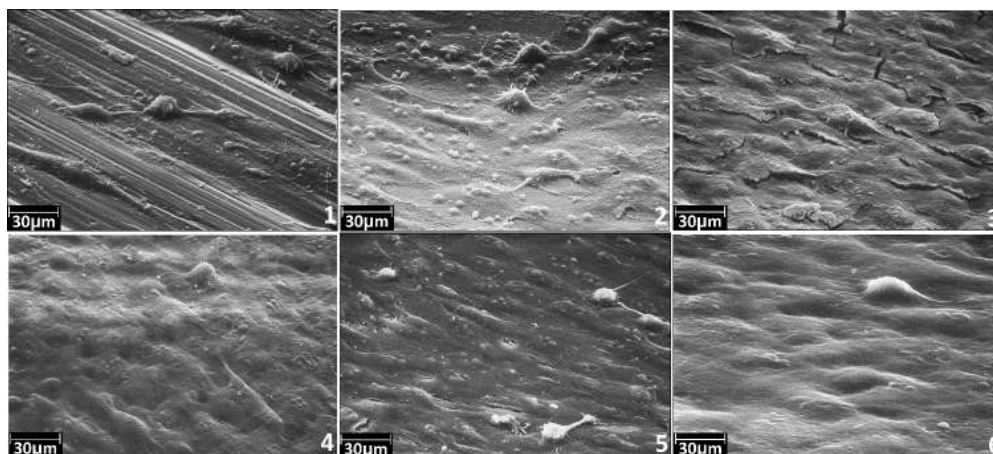


Figure 10. Characteristic SEM images for the samples No. 1–6 after adhesion and spreading of the human osteoblasts MG-63: (1) polished coarse grained titanium; (2) polished nanotitanium; (3) nanotitanium etched in NH₄OH/H₂O₂-15 min; (4) nanotitanium etched in NH₄OH/H₂O₂-15 min and TiO₂ coated by ALD; (5) nanotitanium etched in H₂SO₄/H₂O₂-15 min; and (6) nanotitanium etched in H₂SO₄/H₂O₂-15 min and TiO₂ coated by ALD.

Despite the fact that the cells concentration was uniform while coating the samples, the surface of Sample 1 (coarse grained titanium) contains single cells. It can indicate low adhesion properties of this sample for the studied cell line. For the Sample 2 (nanotitanium), adhesion is stronger for this kind

of cells. The more adhesive surface for this cells type is found for the nanotitanium sample etched in basic Piranha for 15 min (Sample 3) as well as one etched in acid Piranha for 15 min (Sample 5).

The nanotitanium etched and subsequently coated by 20 nm titania layers (Samples 4 and 6) possesses the most adhesive surface for this cells type. The cells form the uniform monolayer, without clear morphology changes.

It can be preliminarily summarized from the SEM experiments that the most adhesive surface for cultivation of cell line MG-63 is formed from etched nanotitanium subsequently covered by 20 nm TiO₂ layer.

4. Conclusions

In this work, we have demonstrated the opportunity of preparation of a nanotitanium-based bioactive material using integrated approach. The integrated approach included three methods: severe plastic deformation (SPD), chemical etching and atomic layer deposition (ALD).

For the first time, it has been shown experimentally that the nature of the etchant and the etching time have a significant impact on the nanotitanium surface morphology at nano- and microscale. The nanoscale structures such as “mesh”, “sponge”, “coral” or “disordered, developed relief” can be obtained by chemical etching using various type of etchant (acidic or basic Piranha solutions) and exposure time. At the microscale, the pits can be obtained with the diameter 1–2 μm.

On the surface of these structures, crystalline coating of titanium oxide about 20 nm thickness has been successfully deposited by ALD. It was shown that after coating the relief of samples is completely retained at the microscale and only partially at the nanoscale. The data on evaluation of adhesive and spreading properties of the human osteoblasts MG-63 cell culture showed that the samples etching in both Piranha solution and subsequently coated with TiO₂ films have the much better adhesive and spreading properties than untreated ones. Thus, it was shown that integrated approach is available to prepare biocompatible and bioactive material.

Acknowledgments: The authors would like to acknowledge the Russian Ministry of Science and Education for financial support through megagrant No. 14.B25.31.0017. This work was also supported in part by a grant from the St-Petersburg State University, No. 12.37.433.2015. This research was conducted using the equipment of the resource centers of the Research Park of the St. Petersburg State University “Innovative Technologies of Composite Nanomaterials”, Centre for “Physical Methods of Surface Investigation”, Centre for “X-ray Diffraction Studies”, and “Nanotechnology Interdisciplinary Centre”.

Author Contributions: Denis V. Nazarov performed chemical etching, deposition of coatings and material characteristics measurement; Elena G. Zemtsova supervised the project and edited the manuscript; Ruslan Z. Valiev provide the samples of nanostructured titanium for etching and edited the manuscript; and Vladimir M. Smirnov conceived the work flow and experiments and prepared the initial draft of the manuscript.

Conflicts of Interest: The authors declare no conflict of interest.

References

1. Brunette, D.M.; Tengvall, P.; Textor, M.; Thomsen, P. (Eds.) *Titanium in Medicine: Material Science, Surface Science, Engineering, Biological Responses, and Medical Applications*; Springer-Verlag Berlin Heidelberg: New York, NY, USA, 2001; pp. 1–1019.
2. Geetha, M. Ti based biomaterials, the ultimate choice for orthopaedic implants—A review. *Prog. Mater. Sci.* **2009**, *54*, 397–425. [[CrossRef](#)]
3. Li, Y.; Yang, C.; Zhao, H.; Qu, S.; Li, X.; Li, Y. New developments of Ti-based alloys for biomedical applications. *Materials* **2014**, *7*, 1709–1800. [[CrossRef](#)]
4. Elias, C.N.; Lima, J.H.C.; Valiev, R.Z.; March, M.A. Biomedical applications of titanium and its alloys. *JOM* **2008**, *60*, 46–49. [[CrossRef](#)]
5. Xie, K.Y.; Wang, Y.; Zhao, Y.; Chang, L.; Wang, G.; Chen, Z.; Cao, Y.; Liao, X.; Lavernia, E.J.; Valiev, R.Z.; *et al.* Nanocrystalline β-Ti alloy with high hardness low Young’s modulus and excellent *in vitro* biocompatibility for biomedical applications. *Mater. Sci. Eng. C* **2013**, *33*, 3530–3536. [[CrossRef](#)] [[PubMed](#)]

6. Lowe, T.C.; Valiev, R.Z. Frontiers for bulk nanostructured metals in biomedical applications. In *Advanced Biomaterials and Biodevices*; Tiwari, A., Nordin, A.N., Eds.; John Wiley & Sons, Inc.: Hoboken, NJ, USA, 2014; pp. 1–52.
7. Valiev, R.Z.; Zhilyaev, A.P.; Langdon, T.G. *Bulk Nanostructured Materials: Fundamentals and Applications*; John Wiley & Sons, Inc: Hoboken, NJ, USA, 2014; pp. 1–440.
8. Hench, L.L.; Jones, J.R. *Biomaterials, Artificial Organs and Tissue Engineering*; Woodhead Publishing Limited: Cambridge, UK, 2005; pp. 15–25.
9. Kulkarni, M.; Mazare, A.; Gongadze, E.; Perutkova, Š.; KraljIglič, V.; Milošev, I.; Schmuki, P.; Iglič, A.; Mozetič, M. Titanium nanostructures for biomedical applications. *Nanotechnology* **2015**, *26*, 062002. [[CrossRef](#)] [[PubMed](#)]
10. Li, B.E.; Li, Y.; Min, Y.; Hao, J.Z.; Liang, C.Y.; Li, H.P.; Wang, G.C.; Liu, S.M.; Wang, H.S. Synergistic effects of hierarchical hybrid micro/nanostructures on the biological properties of titanium orthopaedic implants. *RSC Adv.* **2015**, *5*, 49552–49558. [[CrossRef](#)]
11. Liu, X.; Chu, P.K.; Ding, C. Surface modification of titanium, titanium alloys, and related materials for biomedical applications. *Mater. Sci. Eng. R Rep.* **2004**, *47*, 49–121. [[CrossRef](#)]
12. Bauer, S.; Schmuki, P.; von der Mark, K.; Park, J. Engineering biocompatible implant surfaces Part I: Materials and surfaces. *Prog. Mater. Sci.* **2013**, *58*, 261–326. [[CrossRef](#)]
13. Grigal, I.P.; Markeev, A.M.; Gudkova, S.A.; Chernikova, A.G.; Mityaev, A.S.; Alekhin, A.P. Correlation between bioactivity and structural properties of titanium dioxide coatings grown by atomic layer deposition. *Appl. Surf. Sci.* **2012**, *258*, 3415–3419. [[CrossRef](#)]
14. Yang, B.; Uchida, M.; Kim, H.M.; Zhang, X.; Kukubo, T. Preparation of bioactive titanium metal via anodic oxidation treatment. *Biomaterials* **2004**, *25*, 1003–1010. [[CrossRef](#)]
15. Roy, P.; Berger, S.; Schmuki, P. TiO₂ nanotubes: Synthesis and applications. *Angew. Chem. Int. Ed.* **2011**, *50*, 2904–2939. [[CrossRef](#)] [[PubMed](#)]
16. Vercaigne, S.; Wolke, J.G.C.; Naert, I.; Jansen, J.A. Histomorphometrical and mechanical evaluation of titanium plasma-spray-coated implants placed in the cortical bone of goats. *J. Biomed. Mater. Res.* **1998**, *41*, 41–48. [[CrossRef](#)]
17. Lee, B.H.; Kim, J.K.; Kim, Y.D.; Choi, K.; Lee, K.H. *In vivo* behavior and mechanical stability of surface modified titanium implants by plasma spray coating and chemical treatments. *J. Biomed. Mater. Res.* **2004**, *69*, 279–285. [[CrossRef](#)] [[PubMed](#)]
18. Baryshnikova, M.; Filatov, L.; Mishin, M.; Kondrateva, A.; Alexandrov, S. Formation of hydroxylapatite on CVD deposited titania layers. *Phys. Status Solidi C* **2015**, *12*, 918–922. [[CrossRef](#)]
19. Chen, X.; Mao, S.S. Titanium dioxide nanomaterials: Synthesis, properties, modifications and applications. *Chem. Rev.* **2007**, *107*, 2891–2959. [[CrossRef](#)] [[PubMed](#)]
20. Arbenin, A.Y.; Zemtsova, E.G.; Valiev, R.Z.; Smirnov, V.M. Characteristics of the synthesis of TiO₂ films on a titanium surface by the sol-gel technique. *Russ. J. Gen. Chem.* **2014**, *84*, 2453–2454. [[CrossRef](#)]
21. George, S.M. Atomic layer deposition: An overview. *Chem. Rev.* **2010**, *110*, 111–131. [[CrossRef](#)] [[PubMed](#)]
22. Miikkulainen, V.; Leskelä, M.; Ritala, M.; Puurunen, R.L. Crystallinity of inorganic films grown by atomic layer deposition: Overview and general trends. *J. Appl. Phys.* **2013**, *113*, 021301. [[CrossRef](#)]
23. Hämäläinen, J.; Ritala, M.; Leskelä, M. Atomic layer deposition of noble metals and their oxides. *Chem. Mater.* **2014**, *26*, 786–801. [[CrossRef](#)]
24. Nazarov, D.V.; Bobrysheva, N.P.; Osmolovskaya, O.M.; Smirnov, V.M.; Osmolovsky, M.G. Atomic layer deposition of tin oxide nanofilms: A review. *Rev. Adv. Mater. Sci.* **2015**, *40*, 262–275.
25. Tynell, T.; Karppinen, M. Atomic layer deposition of ZnO: A review. *Semicond. Sci. Technol.* **2014**, *29*, 043001. [[CrossRef](#)]
26. Osmolovskaya, O.M.; Smirnov, V.M. Growth mechanism of nanodimensional vanadium dioxide on silicon surface obtained by ML-ALD method. *Rev. Adv. Mater. Sci.* **2011**, *27*, 184–188.
27. Dendooven, J.; Devloo-Casier, K.; Ide, M.; Grandfield, K.; Kurttepel, M.; Ludwig, K.F.; Bals, S.; van der Voort, P.; Detaverniera, C. Atomic layer deposition-based tuning of the pore size in mesoporous thin films studied by *in situ* grazing incidence small angle X-ray scattering. *Nanoscale* **2014**, *6*, 14991–14998. [[CrossRef](#)] [[PubMed](#)]

28. Zemtsova, E.G.; Arbenin, A.Y.; Plotnikov, A.F.; Smirnov, V.M. Pore radius fine tuning of a silica matrix (MCM-41) based on the synthesis of alumina nanolayers with different thicknesses by atomic layer deposition. *J. Vac. Sci. Technol. A* **2015**, *33*, 021519. [[CrossRef](#)]
29. Hwang, C.S.; Yoo, C.Y. *Atomic Layer Deposition for Semiconductors*; Springer: New York, NY, USA, 2013; pp. 1–263.
30. O'Neill, B.J.; Jackson, D.H.K.; Lee, J.; Canlas, C.; Stair, P.C.; Marshall, C.L.; Elam, J.W.; Kuech, T.F.; Dumesic, J.A.; Huber, G.W. Catalyst design with atomic layer deposition. *ACS Catal.* **2015**, *5*, 1804–1825. [[CrossRef](#)]
31. Niu, W.; Li, X.; Karuturi, S.K.; Fam, D.W.; Fan, H.; Shrestha, S.; Wong, L.H.; Tok, A.I.Y. Applications of atomic layer deposition in solar cells. *Nanotechnology* **2015**, *26*, 064001. [[CrossRef](#)] [[PubMed](#)]
32. Wang, X.; Yushin, G. Chemical vapor deposition and atomic layer deposition for advanced lithium ion batteries and supercapacitors. *Energy Environ. Sci.* **2015**, *8*, 1889–1904. [[CrossRef](#)]
33. Finch, D.S.; Oreskovic, T.; Ramadurai, K.; Herrmann, C.F.; George, S.M.; Mahajan, R.L. Biocompatibility of atomic layer-deposited alumina thin films. *J. Biomed. Mater. Res. A* **2008**, *87*, 100–106. [[CrossRef](#)] [[PubMed](#)]
34. Liang, X.; Lynn, A.D.; King, D.M.; Bryant, S.J.; Weimer, A.W. Biocompatible interface films deposited within porous polymers by atomic layer deposition (ALD). *ACS Appl. Mater. Interfaces* **2009**, *1*, 1988–1995. [[CrossRef](#)] [[PubMed](#)]
35. Putkonen, M.; Sajavaara, T.; Rahkila, P.; Xu, L.; Cheng, S.; Niinistö, L.; Whitlow, H.J. Atomic layer deposition and characterization of biocompatible hydroxyapatite thin films. *Thin Solid Films* **2009**, *517*, 5819–5824. [[CrossRef](#)]
36. Patel, S.; Butt, A.; Tao, Q.; Royhman, D.; Sukotjo, C.; Takoudis, C.G. Novel functionalization of Ti-V alloy and Ti-II using atomic layer deposition for improved surface wettability. *Colloids Surf. B Biointerfaces* **2014**, *115*, 280–285. [[CrossRef](#)] [[PubMed](#)]
37. Valiev, R.Z.; Langdon, T.G. Principles of equal-channel angular pressing as a processing tool for grain refinement. *Prog. Mater. Sci.* **2006**, *51*, 881–981. [[CrossRef](#)]
38. Moulder, J.F.; Stickle, W.F.; Sobol, P.E.; Bomben, K.D. *Handbook of X-ray Photoelectron Spectroscopy: A Reference Book of Standard Spectra for Identification and Interpretation of XPS Data*, 2nd ed.; Physical Electronics, Inc.: Eden Prairie, MN, USA, 1995; pp. 1–261.
39. Vetrone, F.; Variola, F.; de Oliveira, P.T.; Zalzal, S.F.; Yi, J.H.; Sam, J.; Bombonato-Prado, K.F.; Sarkissian, A.; Perepichka, D.F.; Wuest, J.D.; *et al.* Nanoscale oxidative patterning of metallic surfaces to modulate cell activity and fate. *Nano Lett.* **2009**, *9*, 659–665. [[CrossRef](#)] [[PubMed](#)]
40. Variola, F.; Brunski, J.B.; Orsini, G.; Tambasco de Oliveira, P.; Wazen, R.; Nanci, A. Nanoscale surface modifications of medically relevant metals: State-of-the art and perspectives. *Nanoscale* **2011**, *3*, 335–353. [[CrossRef](#)] [[PubMed](#)]
41. D'jkonov, G.S.; Stenina, E.V.; Sviridova, E.V.; Salimgareeva, G.C.; Semenova, I.P.; Zemtsova, E.G.; Valiev, R.Z. Regulation of the surface microrelief of coarse-grained and ultrafine-grained titanium by etching method. *Mater. Phys. Mech.* **2014**, *21*, 259–265.
42. Solovyev, A.A.; Ovchinnikov, D.V.; Korostelev, E.V.; Markeev, A.M. Correlation between structural and bioactive properties of titanium dioxide formed by atomic layer deposition. *Nanotechnol. Russ.* **2013**, *8*, 388–391. [[CrossRef](#)]
43. He, J.; Zhou, W.; Zhou, X.; Zhong, X.; Zhang, X.; Wan, P.; Zhu, B.; Chen, W. The anatase phase of nanotopography titania plays an important role on osteoblast cell morphology and proliferation. *J. Mater. Sci. Mater. Med.* **2008**, *19*, 3465–3472. [[CrossRef](#)] [[PubMed](#)]



© 2015 by the authors; licensee MDPI, Basel, Switzerland. This article is an open access article distributed under the terms and conditions of the Creative Commons Attribution (CC-BY) license (<http://creativecommons.org/licenses/by/4.0/>).